remote sensing

MDPI

Technical Note

Telescopic Network of Zhulong for Orbit Determination and Prediction of Space Objects

Xiangxu Lei [1,2,3], Zhendi Lao [1], Lei Liu [4], Junyu Chen [5], Luyuan Wang [6,*], Shuai Jiang [7] and Min Li [3]

1 School of Civil Engineering and Geomatics, Shandong University of Technology, Zibo 255000, China; xxlei@whu.edu.cn (X.L.); sdutlaozd@163.com (Z.L.)
2 National Astronomical Observatories, Chinese Academy of Sciences, Beijing 100101, China
3 State Key Laboratory of Geodesy and Earth's Dynamics, Innovation Academy for Precision Measurement Science and Technology, Chinese Academy of Sciences, Wuhan 430077, China; limin@whigg.ac.cn
4 School of Geodesy and Geomatics, Wuhan University, Wuhan 430079, China; lliu@sgg.whu.edu.cn
5 Faculty of Land Resources Engineering, Kunming University of Science and Technology, Kunming 650093, China; jychen@kust.edu.cn
6 University of Science and Technology of China, Hefei 230026, China
7 Institute of Spacecraft System Engineering, Beijing 100094, China; jiangshuai13@mails.ucas.ac.cn
* Correspondence: wang_luyuan@sina.com

Abstract: The increasing proliferation of space debris, intermittent space incidents, and the rapid emergence of massive LEO satellite constellations pose significant threats to satellites in orbit. Ground-based optical observations play a crucial role in space surveillance and space situational awareness (SSA). The Zhulong telescopic observation network stands as a pivotal resource in the realm of space object tracking and prediction. This publicly available network plays a critical role in furnishing essential data for accurately delineating and forecasting the orbit of space objects in Earth orbit. Comprising a sophisticated array of hardware components including precise telescopes, optical sensors, and image sensors, the Zhulong network synergistically collaborates to achieve unparalleled levels of precision in tracking and observing space objects. Central to the network's efficacy is its ability to extract positional information, referred to as angular data, from consecutive images. These angular data serve as the cornerstone for precise orbit determination and prediction. In this study, the CPF (Consolidated Prediction Format) orbit serves as the reference standard against which the accuracy of the angular data is evaluated. The findings reveal that the angular data error of the Zhulong network remains consistently below 3 arcseconds, attesting to its remarkable precision. Moreover, through the accumulation of angular data over time, coupled with the utilization of numerical integration and least squares methods, the Zhulong network facilitates highly accurate orbit determination and prediction for space objects. These methodologies leverage the wealth of data collected by the network to extrapolate trajectories with unprecedented accuracy, offering invaluable insights into the behavior and movement of celestial bodies. The results presented herein underscore the immense potential of electric optic telescopes in the realm of space surveillance. By harnessing the capabilities of the Zhulong network, researchers and astronomers can gain deeper insights into the dynamics of space objects, thereby advancing our understanding of the cosmos. Ultimately, the Zhulong telescopic observation network emerges as a pioneering tool in the quest to unravel the mysteries of the universe.

Keywords: space object; telescope; angle measurement; orbit determination; orbit prediction

Citation: Lei, X.; Lao, Z.; Liu, L.; Chen, J.; Wang, L.; Jiang, S.; Li, M. Telescopic Network of Zhulong for Orbit Determination and Prediction of Space Objects. *Remote Sens.* **2024**, *16*, 2282. https://doi.org/10.3390/rs16132282

Academic Editor: Jonathan H. Jiang

Received: 8 April 2024
Revised: 9 June 2024
Accepted: 18 June 2024
Published: 22 June 2024

1. Introduction

The field of space exploration has experienced rapid growth in recent years, with an increasing number of satellites and other space objects being launched into orbit [1,2]. This surge in satellite launches has led to a proliferation of space debris objects orbiting Earth, heightening the risk of collisions for both active and passive spacecraft operating in the low

Earth orbit (LEO) region [3,4]. The precise orbit determination (OD) and orbit prediction (OP) of space objects have become crucial for collision avoidance, space debris mitigation, and efficient spacecraft operations [5].

Before conducting precise OD and OP of space objects, it is necessary to acquire space object orbit measurement data, which primarily consist of the following:

(1) GNSS (Global Navigation Satellite System) data: The fundamental measurement data collected by the onboard GNSS receiver are the pseudo-range or carrier phase data [6]. Satellite orbit data can be obtained through single-point positioning or relative positioning methods [7]. Depending on the data used and the data processing methods, the orbit's accuracy ranges from tens of meters to millimeters [8,9]. GNSS measurement data have high accuracy and can be obtained continuously, round the clock [10]. However, only a limited number of space objects can provide GNSS data.
(2) Radar observation data: Radar systems utilize electromagnetic waves to transmit and receive reflected waves, enabling the determination of the object's position and motion information [11]. Radar systems possess high accuracy and sensitivity, but their regular operation is typically expensive and not readily available to the public.
(3) Telescope angular data: Telescope angular data are obtained by ground or space telescopes through image processing [12]. When the reflected light or radiation from a space object enters the telescope's field of view, it can be detected by the sensor, allowing for the extraction of the object's position information from the captured image. In precision OD and OP, it is usually necessary to extract this positional information and convert it to the desired coordinate system, such as the right ascension/declination or elevation/azimuth coordinate system.

Angle data are an important type of measurement data for precise OD and OP of space objects [13]. The accuracy of angle data is related to image resolution and other factors, typically measured in arcseconds. For instance, at a distance of 1000 km from the telescope, an arcsecond corresponds to approximately 5 m. For example, the angular data obtained by the optical telescope at Mount Stromlo in Australia have an error of less than 1.5 arcseconds [14]. There are also some similar small optical telescopes, such as Changchun LEO EA [15], Changchun GEO EA [16], Falcon [17], OWL-Net [18], FocusGEO [19], SSON [20], AGO70 [21], and APOSOS [22]. Observation using telescopes requires that the space object be illuminated by the sun. The observation is limited by various factors, including weather conditions, the relative position of the space object and the observation platform, the size of the object, and the performance of the telescope. Most angular data for LEO are sparse, with sparsity manifested in two aspects: firstly, the duration of angular data is less than 1% of the orbital period, and the duration of angular data is related to the field of view (FoV) of the telescope, its working mode (tracking, scanning), and space object altitude; secondly, the time interval between two angular arcs is usually large. For example, a study of the angular arc data of 3388 space objects from a telescope in Changchun over a month showed that the average time interval between two angular arc data for the same object was approximately 3 days [23]. Due to limited angular arc data, the process of determining the orbit of a space object often cannot accurately estimate empirical acceleration and struggles to estimate ballistic coefficients. As a result, it absorbs atmospheric mass density model errors. This results in errors of several kilometers when predicting the orbit of the LEO objects for several days with limited angular arc data [15,24,25].

The Zhulong telescopic observation network provides a cost-effective and efficient method for acquiring orbital measurement data of space objects, enabling space scientists globally to share and utilize these data. The network's angular data enable more accurate prediction of the orbits of space objects, which is crucial for avoiding space collisions, assessing the impact of space debris, and studying astrophysics [26].

The following texts introduce the fundamental information about the Zhulong observation network. Then, the accuracy of angular arc data is assessed using CPF (Consolidated Prediction Format) orbital data. Finally, accurate OD and OP measurements are conducted using angular measurement data. The conclusion is at the end of the article.

2. Data and Methods

2.1. Observation Data

The Zhulong observation network is an integrated system of 15 cm telescopes, consisting of more than 9 telescope systems (Figure 1). It has been working steadily since February 2023. The telescope uses a camera and processor integration method to achieve remote control of the filming process, unattended operation, and automatic management of the entire work process based on environmental status information provided by meteorological sensors. This includes dome opening and closing, object search tracking, and recognition positioning. The design parameters are as follows:

(1) FoV: 6.5° × 6.5°;
(2) Aperture: 150 mm;
(3) Detection ability: 15 stars (under 20-star sky brightness);
(4) Photometric accuracy: better than 0.3 magnitudes in star brightness.

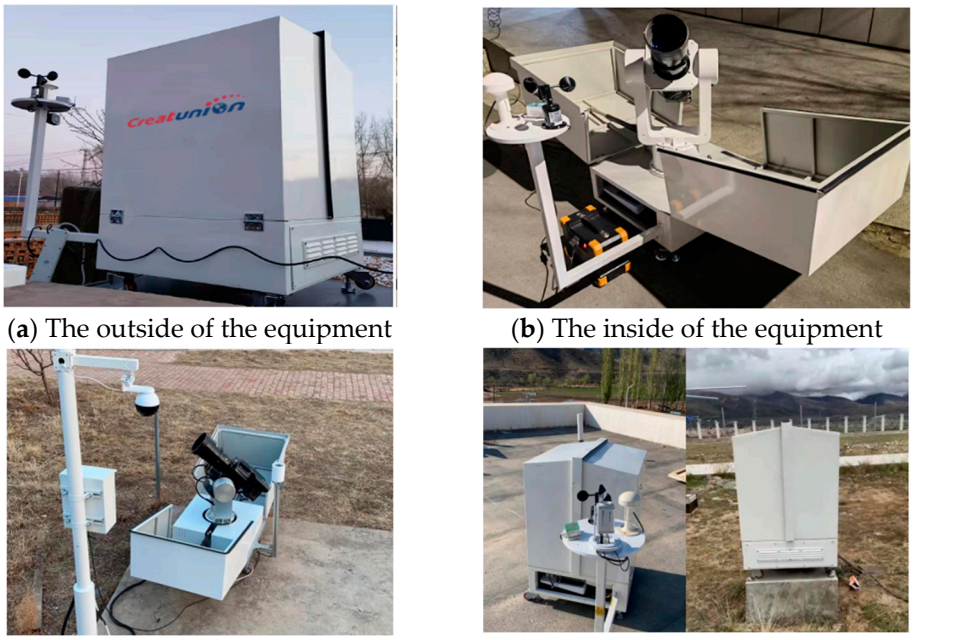

(**a**) The outside of the equipment (**b**) The inside of the equipment

(**c**) The telescope and the monitor (**d**) The equipment with different perspectives

Figure 1. A telescope observation system in Zhulong.

Under suitable observation conditions, LEO space objects can be tracked at a rate of 31 to 201 objects per day, with a sampling frequency of approximately 1 Hz and an average arc length of about 86 s.

The direct data obtained through the telescope system are images, and continuous image information can be obtained through astronomical positioning technology to generate angle measurement data. Astronomical positioning refers to the process of providing a set of space object observation images, along with information about the observation time epoch and equipment pointing. It involves using star position estimation to determine the right ascension/declination or pitch/yaw of the celestial object at the moment of observation, thus forming a time series of angle measurements for the celestial object [27]. The core of astronomical positioning lies in how to correctly identify stars in the image and determine their location information, also known as star identification. Once the star identification is completed, the right ascension/declination of the space object can be determined using the right ascension/declination of the stars. It should be noted that the accuracy of the determined space object angle data ultimately depends on factors such as the accuracy of the image object's centroid position, the number and distribution of stars, the field of view, and the aspect ratio of the charge-coupled device (CCD) camera. The

website not only provides image data for monitoring space objects but also provides their angle data.

2.2. CPF Data

Various sources of errors in telescopes, such as optical distortion, instrumental noise, and atmospheric turbulence, can affect the accuracy of angular data. This section will aggregate observation files spanning multiple days for three celestial bodies. It will utilize precise CPF orbits as reference orbits. These orbits will be compared with angular data to quantify differences. Subsequently, an analysis of angular data accuracy will be conducted.

Three space objects have been chosen, and their NORAD (North American Aerospace Defense Command) numbers, orbital information, and names are provided in Table 1. The table presents the calculated orbital period, inclination, perigee height, and apogee height based on the data from October 2023. Please note that the orbital period is measured in minutes, the inclination is measured in degrees, and the perigee height and apogee height are measured in kilometers, with all data dates falling within 2023.

Table 1. Selected space object information.

NORAD ID	Name	Size/m	Period	Inclination/deg	Apogee/km	Perigee/km	File Count	Start Date	End Date
41240	JASON 3	1 × 1 × 3.7	112.42	66.04	1344	1332	16	June 27th	October 5th
46984	S6 MICHAEL FREILICH	5.13 × 4.17 × 2.34	112.42	66.04	1344	1332	14	June 17th	October 7th
1328	EXPLORER 27	~2.3 × 2.3	107.56	41.18	1303	924	8	July 23rd	September 30th

To evaluate the accuracy of the angular measurements for the three chosen space objects, 38 sets of angular arc files from mid-June to early October 2023 were collected. The reference orbit used is ephemeris files in CPF. CPF serves as a predictive format offered by the International Laser Ranging Service (ILRS), facilitating the dissemination of precise orbit prediction data concerning more than 100 SLR satellites. Its purpose extends to furnishing guidance for satellite laser ranging operations [21]. Each CPF file contains the satellite's position information at regular time intervals over several days, usually in the form of x, y, and z coordinates in a geocentric coordinate system. Currently, more than 30 institutions provide CPF for various satellites [22]. CPF files are usually created using satellite laser ranging data, and their accuracy is affected by factors such as the distribution and precision of the data, the satellite orbit altitude, the geometric characteristics of the satellite, and the precise orbit determination strategy used for the laser ranging data [28–30]. Typically, the accuracy of the CPF is considered to be within several meters [31–33]. The format of CPF varies for different satellites but generally includes three parts: a header, data records, and end-of-file identification. The orbits of the three selected space objects have a precision of approximately 2 m, which is adequate for evaluating the accuracy of angular data with an objected precision of 3 arc seconds.

The method for analyzing the accuracy of angular data is as follows:

(1) Data collection and preprocessing. Register on the website https://spacemapper.cn/ (accessed on 1 June 2024). and download the angular data for selected objects. Download the CPF files for the objects from the ILRS website at the time of the angular data. Perform outlier detection and remove any outliers.

(2) Reference angular data generation. According to the telescopic position and time provided in the angular data file, the method for calculating the reference angular data using the reference orbit is as follows: First, the three-dimensional coordinates obtained from the CPF file are denoted as $\vec{r}_t = \begin{bmatrix} x_t \\ y_t \\ z_t \end{bmatrix}$. Second, based on the telescopic

position $\vec{\boldsymbol{R}}_t = \begin{bmatrix} X_t \\ Y_t \\ Z_t \end{bmatrix}$, the right ascension ($\varnothing_r$) of the space object, declination (δ_r), and calculation formulas are

$$\varnothing_r = \arctan(\Delta Y_t / \Delta X_t) \quad (1)$$

$$\delta_r = \arcsin(\Delta Z_t / \rho_t) \quad (2)$$

where

$$\Delta X_t = x_{t-\Delta t} - X_t$$
$$\Delta Y_t = y_{t-\Delta t} - Y_t$$
$$\Delta Z_t = z_{t-\Delta t} - Z_t$$

$$\rho_t = \sqrt{\Delta X_t{}^2 + \Delta Y_t{}^2 + \Delta Z_t{}^2}$$

$$\widetilde{\rho}_t = \sqrt{(x_t - X_t)^2 + (y_t - Y_t)^2 + (z_t - Z_t)^2}$$

Among them, $\varnothing_r$ represents the reference right ascension, and δ_r represents the reference declination. c refers to the speed of light. Note that $x_{t-\Delta t}$, $y_{t-\Delta t}$, and $z_{t-\Delta t}$ represent the position of a space object, accounting for the propagation speed of photons, and are calculated using Lagrange interpolation polynomials. In addition, all data's time and coordinate systems need to be consistent.

(3) Angular data error calculation. For a certain moment, the error of angular data is defined as

$$\Delta\varnothing = \varnothing_o - \varnothing_r \quad (3)$$

$$\Delta\delta = \delta_o - \delta_r \quad (4)$$

$$e = \sqrt{(\varnothing_o - \varnothing_r)^2 + (\delta_o - \delta_r)^2} \quad (5)$$

where $\varnothing_o$ refers to the observed right ascension and δ_o refers to the observed declination. The error e is calculated using Equation (5). The standard deviation S of an angular data file with n sets is given by Equation (6).

$$S = \sqrt{\sum_{i=1}^{n} (e_i - \bar{e})^2 / (n-1)} \quad (6)$$

where e_i refers to the error of each angular data point and $\bar{e}$ is its mean value.

Figure 2 presents the error of angular data collected at 21:38:00 on 28 September 2023. The angular data in this file start at 21:38:00 on 28 September 2023, with approximately one data point per second for approximately 3 min.

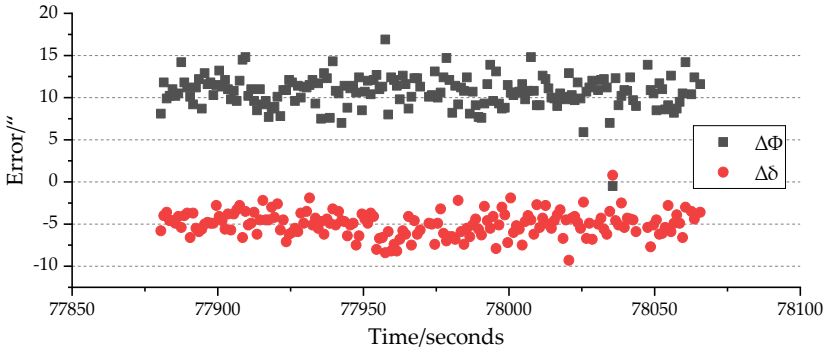

Figure 2. The errors of angular data that occurred on 28 September 2023.

The accuracy of angular data is usually associated with the characteristics of the telescope positions and space objects. Table 2 presents error statistics for 2 stations and 3 space objects. The results show that the accuracy of angular data for the three space objects

and two telescope stations is relatively similar, with an average value of approximately 10 arcseconds and a standard deviation of around 3 arcseconds. In addition, the average error in the right ascension for all files is approximately 2 arcseconds, with a standard deviation of about 7.3 arcseconds. The average error in declination is approximately −3 arcseconds, with a standard deviation of about 3.8 arcseconds.

Table 2. Error statistics for 2 stations.

NORAD ID	Stn6002	Stn 5001	File Count
41240	$\bar{e}$ =11 S =5.2	$\bar{e}$ =10 S =3.4	16
46984	$\bar{e}$ =8 S =3.4	--	14
1328	$\bar{e}$ =10 S =2.6	--	8
All	$\bar{e}$ = 9 S = 3.1	$\bar{e}$ =10 S =3.4	38

-- indicates no data.

2.3. Method of Precision OD and OP

Precise OD can be conducted using continuous multi-day angular arc data. Orbit determination utilizes the least squares estimation method, which calculates an orbit that minimizes the sum of squared residuals between theoretical and actual observations. Set the quantity of the state.

$$\boldsymbol{x} = \{\boldsymbol{r}, \boldsymbol{v}, \boldsymbol{p}\}^T \tag{7}$$

where $\boldsymbol{r}$ and $\boldsymbol{v}$ represent the three-dimensional position and velocity vectors of the orbit, respectively. $\boldsymbol{p}$ is the parameter vector of the force model to be estimated, typically including drag coefficients, pressure of light, etc. Assuming there is a functional relationship between the measured angular data ($\boldsymbol{y}$) and the initial orbit ($\boldsymbol{x_0}$),

$$\boldsymbol{y} = f(\boldsymbol{x_0}) + \boldsymbol{n} \tag{8}$$

where $\boldsymbol{n}$ is the measurement noise. The OD process requires minimizing the weighted sum of squares of the difference between the actual observed value $\boldsymbol{y}$ and the value calculated using the mathematical and physical model $f(\boldsymbol{x_0})$, under the conditions of given angular data $\boldsymbol{y}$, statistical characteristics of the mathematical model f, and noise n.

$$(y - f(\boldsymbol{x_0}))^T P(\boldsymbol{y} - f(\boldsymbol{x_0})) = min \tag{9}$$

Here, P is the weight matrix and the estimated value of $\boldsymbol{x_0}$, denoted as $\hat{\boldsymbol{x}}_0$, is

$$\hat{\boldsymbol{x}}_\mathbf{0} = \boldsymbol{x_0} + \Delta\hat{\boldsymbol{x}}_\mathbf{0} \tag{10}$$

The equation constructed using the least squares principle is

$$(\boldsymbol{A^T P A})\, \Delta\hat{\boldsymbol{x}}_\mathbf{0} = \boldsymbol{A^T P}(\boldsymbol{y} - f(\boldsymbol{x_0})) \tag{11}$$

where $\mathrm{A} = \left(\frac{\partial f}{\partial x}\right)\Big|_{x=x_0}$ is the partial derivative matrix. The solution of the previous equation is

$$\Delta\hat{\boldsymbol{x}}_\mathbf{0} = (\boldsymbol{A^T P A})^{-\mathbf{1}} \boldsymbol{A^T P}(\boldsymbol{y} - f(\boldsymbol{x_0})) \tag{12}$$

The process described above is a continuous iterative process. Initially, $\hat{\boldsymbol{x}}_\mathbf{0}$ is solved and used as an approximation of the initial state quantity. The process is then repeated until the variation of the solved $\hat{\boldsymbol{x}}_\mathbf{0}$ satisfies the condition of convergence, typically when the number of position corrections in the two calculations is less than 1 mm. To obtain an accurate orbit, a set of angular measurements with minimal error is necessary, along with a complete

mathematical model $f(\boldsymbol{x_0})$. Commonly used mathematical models include the Cowell numerical integration model and the Gauss–Jackson model [34]. All subsequent examples use the Cowell model. The force models used in OD and OP include the gravity field JGM-3 50 × 50, third-body gravity, atmospheric mass density model NRLMSISE-00 [35] and JB2008 [36] for atmospheric drag, and solar radiation pressure.

The OP can be described as

$$\begin{cases} \frac{d\boldsymbol{x}}{dt} = f(\boldsymbol{x}, t) \\ \boldsymbol{x}(t_0) = \boldsymbol{x_0} \end{cases} \tag{13}$$

where $\boldsymbol{x}_0$ and f have been obtained in the OD. The orbit at a given moment is

$$\boldsymbol{x}(t) = \boldsymbol{x}(t_0, \boldsymbol{x_0}; t) \tag{14}$$

The form of the OD and OP results is similar to that of the CPF file, i.e., the position and velocity of the space object are given at certain time intervals.

3. Results

After obtaining the OD and OP results, two forms of accuracy assessment can be conducted. One is called internal consistency, which calculates the differences between the determined orbits and the angle observation. The other is external consistency, which compares the differences between the determined orbits and external data, in this case, the CPF orbits. In this section, an analysis of the internal and external consistency of OD's angular measurements for selected space objects, along with the external consistency of OP, will be presented.

The example in Figure 3 utilizes the residuals (differences between observations and orbital determinations) of OD for 41,240 space objects from 4 to 8 July 2023. The example includes two files of angular data from Telescope Stn 5001. One file was recorded at 14:00 UTC on the 4th, and the other was recorded at 13:00 UTC on the 7th, with a time interval of approximately 3 days. The standard deviation of the declination and right ascension differences over the 3 days was calculated to be 1.6.

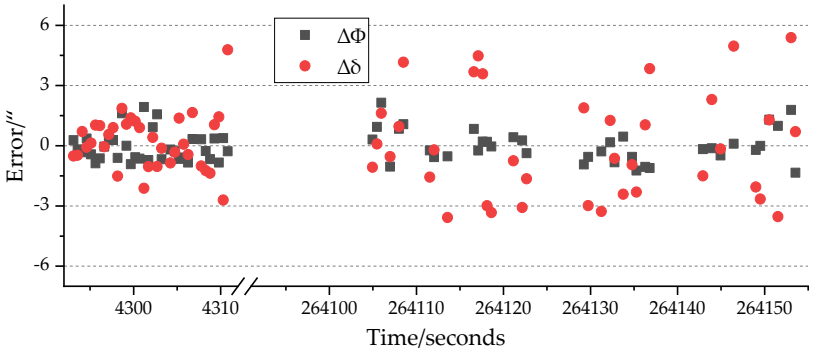

Figure 3. Differences between OD results and angular data starting from 4 July 2023.

Figures 4–7 present the results of precise OD and OP for three space objects using angular data over some time, compared to reference orbits. The results include along-track, radial, and across-track errors and spatial distance differences. The horizontal axis in the figures describes the time in days, with 0 representing the start of the prediction period, negative values corresponding to OD, and positive values corresponding to OP. From the results in the figures, it can be seen that OD can be achieved within a time range of 3 days to 10 days. The comparison of the OD results with the reference orbits shows an error within 800 m. The OP error tends to increase exponentially with time, and this trend is related to many factors, such as the OD error and the force model error. During the OD and OP, the NRLMSISE-00 and JB2008 were utilized. As the orbital altitudes of the three space objects surpassed 1000 km, coupled with the sparsity of angular data, the utilization of both density models in conducting precise OD and OP resulted in similar error outcomes.

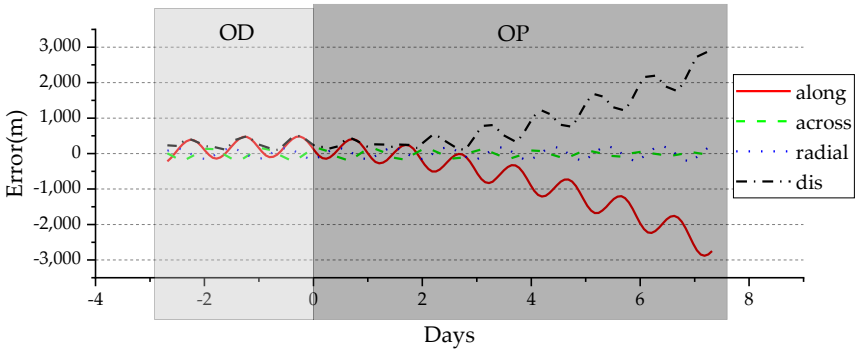

Figure 4. Error of No. 1328 from 23 July 2023.

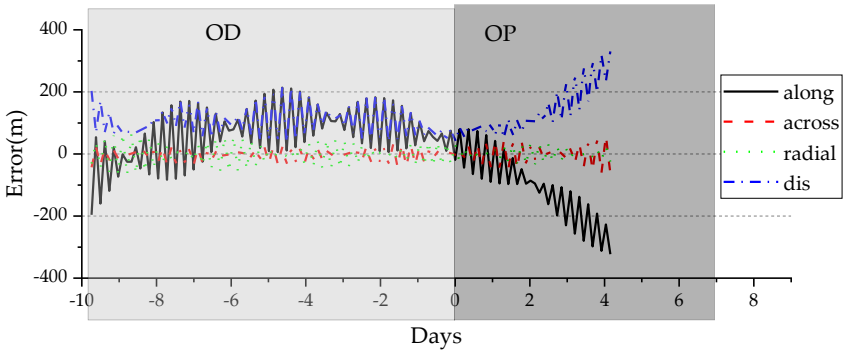

Figure 5. Error of No. 46984 from 16 June 2023.

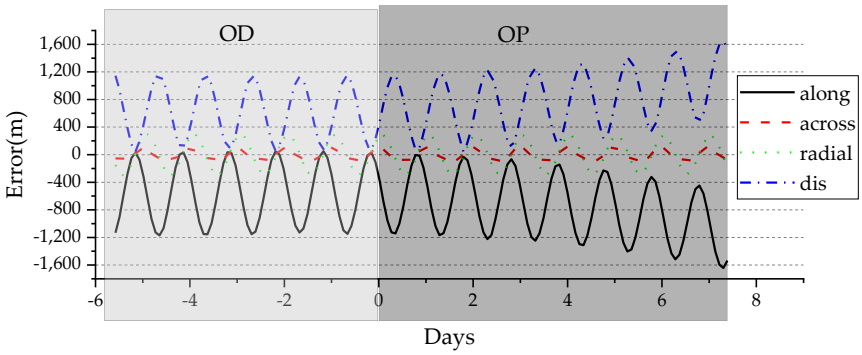

Figure 6. Error of No. 41240 from 3 July 2023 (OD duration 6 days).

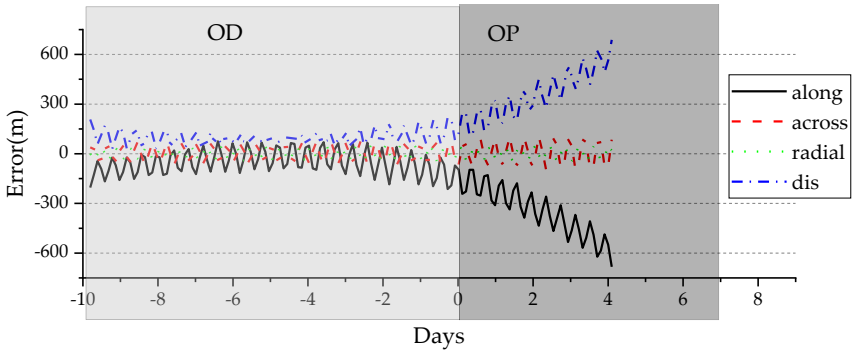

Figure 7. Error of No. 41240 from 3 July 2023 (OD duration 10 days).

Table 3 provides results of the precise OD and OP for the three space objects over three months. The table includes information for each example case, including internal consistency information that compares the OD results with the measured angular data

and differences in the OD and one-day OP compared to the reference orbits. The "No. of observation files" in the table refers to the number of angular data files used in the OD process. Each angular data file contains a complete observation arc, with each case in the table having a data period of approximately 3 min. The results in the table show that at least two angular data files are required during the OD period. The internal consistency errors of OD are all within 3 arcseconds, but the external consistency errors corresponding to similar internal consistency errors vary greatly, with OD errors ranging from tens of meters to over two kilometers. The correlation coefficients of OD errors concerning OP error, the number of angular data files, and OD duration are 0.986, −0.44, and −0.36, respectively.

Table 3. Statistics of outlier coincidence errors in orbit determination prediction.

NORAD ID	OD Start Date in 2023	OD Duration	files Number	OD Fitting Errors/"	OD Errors	1-Day OP Errors
41240	Jul. 3	2	2	2	1703	1842
	Jul. 3	5	3	2	312	352
	Jul. 3	6	4	2	731	742
	Jul. 3	10	6	3	106	212
	Jul. 3	11	7	3	178	314
	Jul. 7	2	2	2	904	1086
	Jul. 12	2	3	2	201	206
	Sep. 25	3	2	2	666	689
	Oct. 4	1	3	2	203	275
46984	Jun. 16	10	2	1	120	129
	Jul. 3	1	3	2	57	218
	Jul. 3	11	4	2	348	480
	Jul. 25	1	2	1	811	1044
	Jul. 25	2	4	2	583	616
	Sep. 26	2	3	2	284	288
	Sep. 26	11	4	2	92	42
1328	Jul. 23	3	2	2	318	395
	Jul. 25	2	2	2	502	503
	Sep. 25	2	3	2	534	549
	Sep. 25	3	4	2	107	109
	Sep. 25	4	5	2	177	179

4. Discussion

(1) Increasing the number of telescope systems

The Zhulong telescopic network is planned to exceed nine telescope systems to obtain more measurement data. If these devices are installed globally, it is possible to obtain continuous observation data for space objects. Multiple telescope systems can simultaneously observe the same space object, enabling the acquisition of more precise data and enabling more accurate applications, such as improving orbit accuracy and establishing space object models [37]. These data will help us to better understand the movement trajectory and possible influence of space objects, making an important contribution to the development of the field of space science.

(2) Improving OP through machine learning

With the rapid development of Artificial Intelligence (AI) and machine learning (ML) technology [38], some research results have been achieved based on historical orbital measurement data, using ML to enhance OP accuracy. However, there is relatively little research on improving the OP of ML based on sparse angle data due to the scarcity of angular data obtained by telescopes. Future research can explore the data conditions (such as accuracy and distribution) under which machine learning can effectively enhance the accuracy of traditional OD and OP. Through in-depth research, valuable insights may be discovered, such as the optimal data conditions for selecting the most suitable ML

method to enhance OP or the data distribution conditions under which ML can effectively improve OP accuracy. Such research will provide us with a deeper understanding of how to effectively utilize sparse data for ML to further improve the accuracy of OP. This will provide an important reference for future calculations of space object orbits and help us better understand the movement trajectory and possible influence of space objects. In comparing the use of machine learning for OD and OP, we have found that the current literature primarily focuses on enhancing the accuracy of OP. Three additional references have been added to the reference list [23,39,40]. Specifically, the first article utilizes Two-Line Element (TLE) data, while the second relies on simulated datasets.

(3) Characterization detection of space objects

Using telescopes, detailed information about space objects can be observed and collected, including their position, velocity, shape, size, and composition. This information is crucial for understanding the characteristics of space objects, their trajectory of movement, and their potential influence. The Zhulong telescopic network can also be used for the characterization detection of space objects. For instance, spectral analysis can help us understand the composition of an object. Brightness changes [41] can provide insights into the object's active state and changes. Measuring position and velocity can help us gain insight into the object's orbit and movement. In the future, with continued technological advancements, scientists anticipate the production of larger and more precise telescopes. These advanced instruments will offer enhanced insights into space objects, providing more detailed information. Additionally, with the advancement in data analysis technology and computer science, these data can be processed and analyzed more effectively to gain a deeper understanding of the mysteries of the universe.

5. Conclusions

Telescope network data on the angular positions of space objects are a crucial type of orbital measurement data. This article provides orbital measurement data from the Zhulong telescopic network, which can be publicly accessed by users worldwide. These data are of great significance for the study of the orbits and other characteristics of space objects. Over three months, we analyzed the angular data of three typical space objects and conducted OD and OP calculations. The angular data accuracy analysis results show that the angular data errors for the selected period of the space objects are less than 3 arcseconds. The precise OD and OP results show that the internal consistency error of the orbit determination is within 3 arcseconds. Secondly, when using the CPF orbits as the reference orbit, the OD and OP errors are generally in the hundreds of meters range. The OD error is closely related to the OD duration and the number of observations passed. If the OD duration remains constant, the more observation passes are used, and the smaller the OD and OP errors become. This result also demonstrates the importance of the Zhulong telescopic network in providing open data for precise OD and OP of space objects.

Author Contributions: Conceptualization, J.C. and X.L.; methodology, J.C.; software, J.C. and L.L.; validation, X.L. and Z.L.; formal analysis, L.L.; investigation, S.J.; resources, L.W.; data curation, J.C.; writing—original draft preparation, X.L.; writing—review and editing, J.C. and M.L.; supervision, J.C.; project administration, L.L.; funding acquisition, M.L., X.L. and J.C. All authors have read and agreed to the published version of the manuscript.

Funding: This research was supported by the National Natural Science Foundation of China (12303081), Shandong Provincial Natural Science Foundation General Project (ZR2023MD098), Yunnan Fundamental Research Projects (202301AT070159), the Open fund of State Key Laboratory of Geodesy and Earth's Dynamics (SKLGED2024-3-5), and the Scientific Innovation Project for Young Scientists in Shandong Provincial Universities (2022KJ224).

Data Availability Statement: The angle data used in the text are available at https://spacemapper.cn/ (accessed on 1 June 2024). Note that this website requires a registered account, and data can be accessed after successful registration. Requests for observations of space objects may also be made, and those that are made are likely to be approved. The data obtained by the Zhulong telescopic

network in the article, such as image data and angular data, were provided by Yaya Li from Beijing Creatunion Parallel Space Technology Co., Ltd. For more information about these data, please refer to the website.

Acknowledgments: We acknowledge and appreciate https://ilrs.gsfc.nasa.gov (accessed on 1 June 2024) for providing the CPF data, which are important accuracy evaluation data in this paper.

Conflicts of Interest: The authors declare no conflicts of interest.

References

1. Metzger, P.T. Space development and space science together, a historic opportunity. *Space Policy* **2016**, *37*, 77–91. [CrossRef]
2. McDowell, J.C. The Low Earth Orbit Satellite Population and Impacts of the SpaceX Starlink Constellation. *Astrophys. J. Lett.* **2020**, *892*, 18. [CrossRef]
3. Greenbaum, D. Space debris puts exploration at risk. *Science* **2020**, *370*, 922. [CrossRef] [PubMed]
4. Guterman, L. Strike creates space debris. *Science* **2021**, *374*, 919.
5. Marty, J.Y.; Bonnal, C.; Faucher, P.; Francillout, L. Space traffic management as a necessity for future orbital operations a French perspective. *Acta Astronaut.* **2023**, *202*, 278–282. [CrossRef]
6. Mosavi, M.R.; Azad, M.S.; EmamGholipour, I. Position Estimation in Single-Frequency GPS Receivers Using Kalman Filter with Pseudo-Range and Carrier Phase Measurements. *Wirel. Pers. Commun.* **2013**, *72*, 2563–2576. [CrossRef]
7. Paziewski, J.; Fortunato, M.; Mazzoni, A.; Odolinski, R. An analysis of multi-GNSS observations tracked by recent Android smartphones and smartphone-only relative positioning results. *Measurement* **2021**, *175*, 16. [CrossRef]
8. Strugarek, D.; Sośnica, K.; Arnold, D.; Jäggi, A.; Zajdel, R.; Bury, G. Satellite laser ranging to GNSS-based Swarm orbits with handling of systematic errors. *GPS Solut.* **2022**, *26*, 16. [CrossRef]
9. Li, X.X.; Chen, X.; Ge, M.; Schuh, H. Improving multi-GNSS ultra-rapid orbit determination for real-time precise point positioning. *J. Geod.* **2019**, *93*, 45–64. [CrossRef]
10. Van Den Ijssel, J.; Encarnação, J.; Doornbos, E.; Visser, P. Precise science orbits for the Swarm satellite constellation. *Adv. Space Res.* **2015**, *56*, 1042–1055. [CrossRef]
11. Leonard, R.; Williams, I.D. Viability of a circular economy for space debris. *Waste Manag.* **2023**, *155*, 19–28. [CrossRef] [PubMed]
12. Schildknecht, T. Optical surveys for space debris. *Astron. Astrophys. Rev.* **2007**, *14*, 41–111. [CrossRef]
13. San Martin, F.I.; Perez, C.A.; Tapia, J.E.; Virani, S.; Holzinger, M.J. Automatic space object detection on all-sky images from a synoptic survey synthetic telescope array. *Adv. Space Res.* **2020**, *65*, 337–350. [CrossRef]
14. Sang, J.; Bennett, J.C.; Smith, C. Experimental results of debris orbit predictions using sparse tracking data from Mt. Stromlo. *Acta Astronaut.* **2014**, *102*, 258–268. [CrossRef]
15. Lei, X.; Li, Z.; Du, J.; Chen, J.; Liu, C. Identification of uncatalogued LEO space objects by a ground-based EO array. *Adv. Space Res.* **2021**, *67*, 350–359. [CrossRef]
16. Yang, W.; Li, Z.W.; Liu, M.; Liu, D.; Sun, J.; Zhang, Z.; Yu, H. Detection approach for GEO space objects with a wide-field optical telescope array. *Opt. Express* **2023**, *31*, 18717–18733. [CrossRef]
17. Chun, F.K.; Tippets, R.D.; Strong, D.M.; Della-Rose, D.J.; Polsgrove, D.E.; Gresham, K.C.; Reid, J.A.; Christy, C.P.; Korbitz, M.; Gray, J.; et al. A new global array of optical telescopes: The falcon telescope network. *Publ. Astron. Soc. Pac.* **2018**, *130*, 095003. [CrossRef]
18. Shin, B.; Lee, E.; Park, S.Y. Determination of Geostationary Orbits (GEO) Satellite Orbits Using Optical Wide-Field Patrol Network (OWL-Net) Data. *J. Astron. Space Sci.* **2019**, *36*, 169–180. [CrossRef]
19. Luo, H.; Zheng, J.H.; Wang, W.; Cao, J.J.; Zhu, J.; Chen, G.P.; Zhang, Y.S.; Liu, C.S.; Mao, Y.D. FocusGEO II. A telescope with imaging mode based on image overlay for debris at Geosynchronous Earth Orbit. *Adv. Space Res.* **2022**, *69*, 2618–2628. [CrossRef]
20. Hossein, S.H.; Acernese, M.; Cardona, T.; Cialone, G.; Mariani, L.; Marini, V.; Marzioli, P.; Parisi, L.; Piergentili, F.; Santoni, F. Sapienza Space debris Observatory Network (SSON): A high coverage infrastructure for space debris monitoring. *J. Space Saf. Eng.* **2020**, *7*, 30–37. [CrossRef]
21. Šilha, J.; Krajčovič, S.; Zigo, M.; Tóth, J.; Žilková, D.; Zigo, P.; Kornoš, L.; Šimon, J.; Schildknecht, T.; Cordelli, E.; et al. Space debris observations with the Slovak AGO70 telescope: Astrometry and light curves. *Adv. Space Res.* **2020**, *65*, 2018–2035. [CrossRef]
22. Guo, X.; Gao, P.; Shen, M.; Yang, D.; Yu, H.; Liu, T.; Li, J.; Zhao, Y. Introduction to APOSOS project: 15 cm aperture elec-tro-optical telescopes to track space objects. *Adv. Space Res.* **2020**, *65*, 1990–2002. [CrossRef]
23. Chen, J.; Sang, J.; Li, Z.; Liu, C. A Case Study on the Effect of Atmospheric Density Calibration on Orbit Predictions with Sparse Angular Data. *Remote Sens.* **2023**, *15*, 3128. [CrossRef]
24. Abdelaziz, A.M.; Ibrahim, M.; Liang, Z.; Dong, X.; Tealib, S.K. Orbit Predictions for Space Object Tracked by Ground-Based Optical and SLR Stations. *Remote Sens.* **2022**, *14*, 13. [CrossRef]
25. Lee, E.; Park, S.Y.; Hwang, H.; Choi, J.; Cho, S.; Jo, J.H. Initial orbit association and long-term orbit prediction for low earth space objects using optical tracking data. *Acta Astronaut.* **2020**, *176*, 247–261. [CrossRef]
26. Du, J.; Chen, j.; Li, B.; Sang, J. Tentative design of SBSS constellations for LEO debris catalog maintenance. *Acta Astronaut.* **2019**, *155*, 379–388. [CrossRef]

27. Zhang, X.; Zhang, Y.; Zhang, C. Random Star Recognition Algorithm Based on Image Total Station and Its Application to Astronomical Positioning. *J. Surv. Eng.* **2022**, *148*, 7. [CrossRef]
28. Pearlman, M.R.; Noll, C.E.; Pavlis, E.C.; Lemoine, F.G.; Combrink, L.; Degnan, J.J.; Kirchner, G.; Schreiber, U. The ILRS: Approaching 20 years and planning for the future. *J. Geod.* **2019**, *93*, 2161–2180. [CrossRef]
29. Noll, C.E.; Ricklefs, R.; Horvath, J.; Mueller, H.; Schwatke, C.; Torrence, M. Information resources supporting scientific research for the international laser ranging service. *J. Geod.* **2019**, *93*, 2211–2225. [CrossRef]
30. Najder, J.; Sosnica, K. Quality of Orbit Predictions for Satellites Tracked by SLR Stations. *Remote Sens.* **2021**, *13*, 20. [CrossRef]
31. Steindorfer, M.A.; Kirchner, G.; Koidl, F.; Wang, P.; Jilete, B.; Flohrer, T. Daylight space debris laser ranging. *Nat. Commun.* **2020**, *11*, 6. [CrossRef]
32. Tang, G.S.; Cao, J.; Liu, S.; Chen, G.; Man, H.; Zhang, X.; Shi, S.; Sun, J.; Li, Y.; Calabia, A. APOD mission status and preliminary results. *Sci. China-Earth Sci.* **2020**, *63*, 257–266. [CrossRef]
33. Luceri, V.; Pirri, M.; Rodríguez, J.; Appleby, G.; Pavlis, E.C.; Müller, H. Systematic errors in SLR data and their impact on the ILRS products. *J. Geod.* **2019**, *93*, 2357–2366. [CrossRef]
34. Montenbruck, O.; Gill, E.; Lutze, F. Satellite orbits: Models, methods, and applications. *Appl. Mech. Rev.* **2002**, *55*, B27–B28. [CrossRef]
35. Picone, J.M.; Hedin, A.E.; Drob, D.P.; Aikin, A.C. NRLMSISE-00 empirical model of the atmosphere: Statistical comparisons and scientific issues. *J. Geophys. Res.* **2002**, *107*, SIA 15-1–SIA 15-16. [CrossRef]
36. Bowman, B.R.; Kent Tobiska, W.; Marcos, F.A.; Valladares, C. The JB2006 empirical thermospheric density model. *J. Atmos. Sol. Terr. Phys.* **2008**, *70*, 774–793. [CrossRef]
37. Anugu, N.; Amorim, A.; Gordo, P.; Eisenhauer, F.; Pfuhl, O.; Haug, M.; Wieprecht, E.; Wiezorrek, E.; Lima, J.; Perrin, G. Methods for multiple-telescope beam imaging and guiding in the near-infrared. *Mon. Not. R. Astron. Soc.* **2018**, *476*, 459–469. [CrossRef]
38. Wurman, P.R.; Stone, P.; Spranger, M. Improving artificial intelligence with games. *Science* **2023**, *381*, 147–148. [CrossRef]
39. Peng, H.; Bai, X. Machine Learning Approach to Improve Satellite Orbit Prediction Accuracy Using Publicly Available Data. *J. Astronaut. Sci.* **2020**, *67*, 762–793. [CrossRef]
40. Li, B.; Huang, J.; Feng, Y.; Wang, F.; Sang, J. A Machine Learning-Based Approach for Improved Orbit Predictions of LEO Space Debris with Sparse Tracking Data from a Single Station. *IEEE Trans. Aerosp. Electron. Syst.* **2020**, *56*, 4253–4268. [CrossRef]
41. Yao, Y.; Zhu, J.; Liu, Q.; Lu, Y.; Xu, X. An Adaptive Space Target Detection Algorithm. *IEEE Geosci. Remote Sens. Lett.* **2022**, *19*, 5. [CrossRef]